Chemical Physics 57 (1981) 45–53
North-Holland Publishing Company

ABSORPTION SPECTRA OF HYDROGEN CYANIDE AND DEUTERIUM CYANIDE IN THE 130–80 nm RANGE

Takashi NAGATA, Tamotsu KONDOW, Yasushi OZAKI and Kozo KUCHITSU
Department of Chemistry, Faculty of Science, The University of Tokyo, Bunkyo-ku, Tokyo 113, Japan

Received 29 October 1980

The absorption spectra of HCN and DCN were measured from 130 to 80 nm. Strong absorption bands were observed below 122 nm both for HCN and DCN. These bands were assigned to the Rydberg series converging to the first and the second ionization potentials and to valence transitions at about 120 and 115 nm. The absorption coefficients for HCN were determined over entire range studied. The maximum absorption coefficient, at 112.39 nm, was measured to be 2.8×10^3 cm^{-1} with an estimated uncertainty of about 20%.

1. Introduction

Since the first measurement of the ultraviolet absorption spectrum of HCN between 200 and 170 nm [1], the absorption spectra of HCN and DCN have been studied extensively in the range 200–130 nm [2–6]. Herzberg and Innes [2] investigated two valence transitions: the $\tilde{A}\,^1A'' \leftarrow \tilde{X}$ system (180–155 nm) for HCN and DCN, and the $\tilde{B}\,^1A'' \leftarrow \tilde{X}$ system (180–155 nm) for DCN†. The third system, $\tilde{C}\,^1A' \leftarrow \tilde{X}$ (155–135 nm) was examined later by Herzberg [3]. Recently, vibrational structures in the $\tilde{C}\,^1A' \leftarrow \tilde{X}$ system were measured by Macpherson and Simons [4] in the 147–130 nm range for the purpose of studying the predissociation of HCN and DCN. Price [5] and Price and Walsh [6] found strong diffuse bands below 112 nm. The absorption spectrum of HCN in the 130–105 nm range was examined by West [7] and by Lee [8] by the use of synchrotron radiation.

Electron energy-loss spectra have also been measured in order to obtain information complementary to that provided by the optical method [9–13]. Taking advantage of the difference in the selection rules existing in electron and photon impact, Chutjian et al. [9] investigated the low-lying triplet and singlet states of HCN by the use of slow electrons. Tam and Brion [10] observed the energy-loss spectrum of HCN and first assigned their spectrum in terms of the Rydberg transitions at energies higher than 10 eV. The work has been followed by Fridh, Åsbrink and Lindholm [11, 12] by electron spectroscopy, by which they have proposed that a valence transition exists below 120 nm in addition to the Rydberg series. The assignments proposed by different groups do not seem to be all consistent. A systematic analysis covering wider wavelength range is needed for a more complete understanding of the HCN and DCN spectra.

The present work is a part of our systematic studies of the photochemistry of HCN and DCN in the vacuum ultraviolet, where various molecular processes such as photodissociation, predissociation and photoionization are expected to proceed. The optical absorption spectra of HCN and DCN were measured and assigned by taking into account the results of electron energy-loss spectroscopy.

2. Experimental

2.1. Apparatus

Fig. 1 shows a schematic diagram of the experimental apparatus. Incident vacuum UV radiation was taken from the electron synchrotron, operated at 1.04 GeV, of the Institute for Nuclear Study, the University of Tokyo. A concave pre-mirror with a radius of curvature of 6 m was used to focus the radiation vertically onto the entrance slit S_1 of a 0.5 m Seya–Namioka monochromator equipped with a concave grating (Bausch and Lomb, Ltd., radius of curvature, 498.1 mm; blaze angle, 2°24'; 1200 grooves/mm). The spectral resolution was ≈0.3 nm or better. Monochromatized radiation from the exit slit S_2 was introduced into an absorption cell. The sample gas was introduced from the end port of the cell and evacuated through the differential slit S_3 of the cell by a 4" diffusion pump having a liquid nitrogen cold trap. The slit S_3 placed in front of the cell was also used as a collimator slit. The pressures of the chamber A and the monochromator B were maintained below 1×10^{-6} Torr and $\approx 2 \times 10^{-6}$ Torr, respectively, during the measurement. The intensity of the radiation before and after the absorption, I_0 and I, respectively, were measured by scintillation counters [14]. The fluorescence from the scintillator (sodium salicylate) was monitored with HTV R374 and R585 photomultipliers for I_0 and I, respectively. Each signal was amplified and fed into a signal divider. The output of the divider, I/I_0, was recorded on a strip chart.

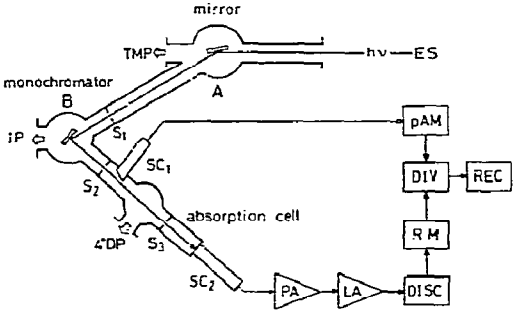

Fig. 1. A schematic drawing of the apparatus. ES: electron synchrotron; TMP: turbe-molecular pump (100 l/s); IP: ionization pump (80 l/s); DP: oil diffusion pump (500 l/s); S_1: entrance slit; S_2: exit slit; S_3: differential slit. SC_1: HTV R374 photomultiplier coated with sodium salicylate used for monitoring I_0. SC_2: HTV R585 photomultiplier coated with sodium salicylate used for measuring I. pAM: pico-ammeter; PA: preamplifier; LA: linear amplifier; DISC: discriminator; RM: ratemeter; DIV: signal divider; REC: strip-chart recorder.

2.2. Sample preparation

The HCN sample was prepared by dropping an aqueous solution of sodium cyanide into sulfuric acid [15]. The HCN gas thus produced was dried on calcium chloride and then purified by vacuum distillation. Deuterium monoxide (D_2O) and D_2SO_4 were used to prepare DCN in a similar way. The isotopic purity of DCN was determined to be about 96% by infrared spectroscopy and by an intensity measurement of the hydrogen Balmer lines produced by electron impact on HCN contaminated in DCN.

2.3. Wavelength calibration

The readings of the monochromator were calibrated against the wavelength of the known absorption spectrum of carbon disulfide (CS_2) in the 100–90 nm range and that of acetylene (C_2H_2) in the 135–110 nm range [16, 17]. These spectra were measured under the identical conditions to those in the HCN and DCN measurements. The wavelengths were calibrated within 20 cm^{-1}. In addition, random statistical errors in individual measurements of HCN and DCN spectra were estimated to be 50 cm^{-1}. Then the overall uncertainty in the absolute value of the wavelength is estimated to be 60 cm^{-1} (one standard deviation). The energies for the transitions determined in the present work agree with those reported by Fridh and Åsbrink [11], whereas those by Tam and Brion [10] are consistently higher than ours by about 160 cm^{-1}.

2.4. Determination of the absorption coefficient

The absorption coefficient k is defined by

$$k = -(1/L_0) \ln (I/I_0), \quad (1)$$

where L_0 is the normalized layer thickness of the sample gas at standard temperature and pressure calculated from the actual length of the absorption cell L (42.5 cm), the gas pressure P and the temperature T (290 K). The sample pressure was monitored with a Pirani gauge soldered on the exit of a gas inlet valve, which was connected to the cell via a copper tube with inner diameter of about 4 mm.

Since the Pirani gauge was separated from the cell by about 50 cm, the pressure in the cell may not be equal to the reading of the gauge, P_g. The pressure of the gas, P, in the cell is assumed to be proportional to P_g,

$$P = \alpha P_g, \quad (2)$$

where α is an instrumental constant. In order to evaluate α, the transmittance, I/I_0, for C_2H_2 at $\approx$105 nm was measured at several different inlet pressures, P_g. The absorption spectrum of C_2H_2 is almost flat and structureless in this wavelength region, where the absorption coefficient is known to be 680 cm^{-1} [18]. By the use of the reported value of k for C_2H_2 together with the given values of L and T, α was calculated to be 0.055 ± 0.009. The uncertainty in α arises from the statistical error in the measured I/I_0 and the reported uncertainty (10–20%) in the k for C_2H_2 [18]. The value of α thus obtained is transferred to the measurement of the absorption coefficients of HCN, because HCN and C_2H_2 are isoelectronic molecules of almost the same size. Difference in the viscosity of HCN and C_2H_2 causes only a small change within experimental error in the values of k. Then the absorption coefficient k is evaluated from eqs. (1) and (2). In fig. 3, the absorption coefficients k for HCN in the 130–80 nm range are shown in a logarithmic scale. The uncertainty in the absolute value of k consists of the fluctuation of I/I_0 in individual measurements and the uncertainty in the values of L_0. The latter mainly arises from the uncertainty in the α constant mentioned above. The overall uncertainty in the absolute value of k is estimated to be $\approx$20% in the spectral range studied. The absorption coefficients for HCN in the present work are 20–30% larger than the values reported by Lee [8] in the 130–105 nm range [8]. If the value of α for HCN is used in the case of DCN, the absorption coefficient k for the most intense peak C in fig. 2b is estimated to be 1.9×10^3 cm^{-1}. This value has a larger experimental error than that for HCN.

3. Results and discussion

The MO calculations [19–22] and the photoelectron spectroscopic studies of HCN [11, 23] show that the electronic configuration of its ground state ($X\ ^1\Sigma^+$) is

$$(1\sigma)^2(2\sigma)^2(3\sigma)^2(4\sigma)^2(5\sigma)^2(1\pi)^4.$$

The first and second ionization potentials obtained from the photoelectron spectra are 13.607 and 14.011 eV, respectively [11]. The former is ascribed to the ionization from the 1π orbital, which is regarded as a bonding π-orbital for the C≡N bond, and the latter to the ionization from the 5σ orbital related primarily to the lone pair electrons of the N atom [22].

As shown in figs. 2a and 3, the absorption spectrum of HCN contains numerous peaks extending from 125 to 90 nm and a broad continuum below 90 nm. Most of the peaks found in this range appear to converge to the continuum. Therefore, these peaks are assigned to the Rydberg series converging to the first and the second ionization limits, 91.1 and 88.4 nm, respectively.

The wavenumber, $\tilde{\nu}$, for a Rydberg transition with a principal quantum number n is calculated by the formula

$$\tilde{\nu} = \mathrm{IP} - R/(n-\delta)^2, \quad (3)$$

where IP is the ionization potential, R is the Rydberg constant and δ is the quantum defect which is characteristic of a given Rydberg series. Several peaks which do not belong to these

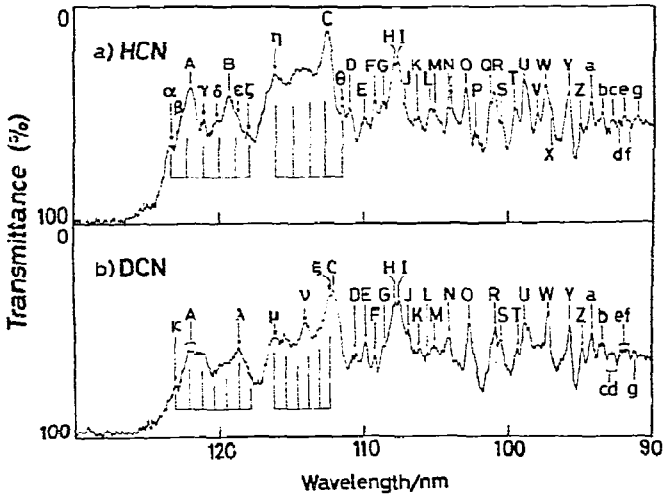

Fig. 2. The absorption spectra of (a) HCN and (b) DCN in the 130–90 nm range. Sample pressures are estimated to be 0.012 Torr for HCN and 0.011 Torr for DCN. Possible vibrational progressions around 120 and 115 nm are indicated by series of lines at regular intervals. Each line indicates an assumed position of the band in the vibrational progressions.

Rydberg series are tentatively assigned to valence transitions. The present assignments are compared with the energy-loss spectra of HCN [10–12]. The assignments for the Rydberg transitions are listed in table 1 and shown in fig. 3.

3.1. Rydberg transitions

3.1.1. $1\pi \rightarrow ns\sigma$ series

The $1\pi \rightarrow ns\sigma$ transitions are optically allowed and should result in intense absorption peaks, because the 1π orbital corresponds to the p_π–p_π

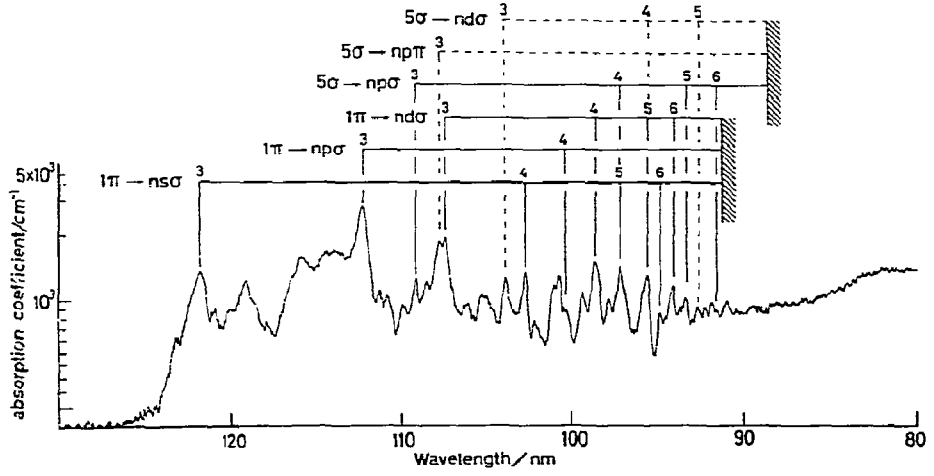

Fig. 3. The absorption spectrum of HCN in the 130–80 nm range. The position of the (000) band for each Rydberg transition is indicated. Tentative assignments for $5\sigma \rightarrow np\pi$ and $5\sigma \rightarrow nd\sigma$ series are indicated by dashed lines. The ordinate shows the absorption coefficient k in a logarithmic scale. See section 2.4.

bonding between the carbon and nitrogen atoms in HCN [22]. If the intense peak A at 121.80 nm in the HCN spectrum (fig. 2a) is assigned to the (000)† band of the first member ($1\pi \rightarrow 3s\sigma$) of the $1\pi \rightarrow ns\sigma$ series, peaks O, W and Z observed at 102.83, 97.35 and 95.04 nm can be assigned to the $n = 4$, 5 and 6 members, respectively. In this case the quantum defect for this series is calculated using eq. (3) to be ≈ 1.05. The quantum defect obtained is comparable with those for the $ns\sigma$ series of the isoelectronic molecules, nitrogen and acetylene and for several small molecules with double or triple bonds [24]. Furthermore, this assignment agrees with that obtained in energy-loss spectroscopy [10–12]. The corresponding peaks are present in the DCN spectrum (see table 1) except for the first member; the peak intensity of this member is diminished, as shown in fig. 2b. The decrease in the intensity of the DCN peak A is probably caused by dissociation, proceeding via the $(1\pi)^3 3s\sigma$ state of DCN. This suggests that the lifetime of the $(1\pi)^3 3s\sigma$ state of DCN is shorter than that of HCN. The line profiles of the HCN and DCN spectra around 120 nm are complex; as discussed in a later section, the origin of this complexity is ascribed to the overlapping of these Rydberg transitions with a progression of bending vibrations inherent to a valence transition.

In the HCN spectrum, two peaks at 119.11 and 100.87 nm, B and R, are assigned to the (001) band of the $1\pi \rightarrow 3s\sigma$ and $4s\sigma$ transitions, respectively, because the wavenumber difference between the (001) and (000) bands of each member is only slightly smaller than 1900 cm^{-1} and is comparable with the wavenumber of the ν_3 mode (≈ 1800 cm^{-1}) of $HCN^+(X\,^2\Pi)$ [11]. The (001) bands of the $1\pi \rightarrow 5s\sigma$ and $6s\sigma$ transitions cannot be assigned unambiguously, because the bands are overlapped with other Rydberg transition peaks. In the DCN spectrum, the (001) band of the $1\pi \rightarrow 3s\sigma$ transition does not appear, probably because of the short lifetime of the $(1\pi)^3 3s\sigma$ state. The (001) band of the $1\pi \rightarrow 4s\sigma$ transition is assigned to peak R at 100.93 nm, which is separated by 1750 cm^{-1} from the (000) band (peak O), as predicted from the wavenumber of the ν_3 mode (≈ 1690 cm^{-1}) for $DCN^+(X\,^2\Pi)$ [11]. On the other hand, the (001) band of the $1\pi \rightarrow 5s\sigma$ transition is uncertain, probably because of overlapping with peaks originating from other Rydberg transitions. The corresponding absorption peak for the $1\pi \rightarrow 6s\sigma$ transition is not well resolved, because of the limited resolution.

3.1.2. $1\pi \rightarrow np\sigma$ series

The peak C at 112.39 nm in the HCN spectrum is the most intense one in the wavelength range studied. This peak is likely to arise from a Rydberg transition, because it has a narrow width characteristic of Rydberg transitions. If this peak is assigned to the (000) band of the first member of the Rydberg series converging to the first ionization potential, the quantum defect is calculated to be 0.70. This value suggests that the transition belongs to the $1\pi \rightarrow np\sigma$ series. If the quantum defect is assumed to be 0.70, the peak S appearing at 100.55 nm can be assigned to the $n = 4$ member. The members of this series with $n \geq 5$ cannot be identified in the HCN spectrum.

In the case of DCN, the corresponding (000) band of the $n = 3$ member, peak C at 112.14 nm, is somewhat broader and has a shoulder on the long wavelength side (see fig. 2b). This indicates that peak C consists of two or more components and results because of the isotope effect. The peak S for $n = 4$ is better separated from peak R because of the isotope shift of peak R, which is already assigned to the (001) band of the $1\pi \rightarrow 4s\sigma$ transition. Then $n = 5$ member appears to exist at about 96.3 nm as a shoulder of peak Y.

In both the HCN and DCN spectra there are three small peaks D, E and G, which can be assigned to vibrational members of the $1\pi \rightarrow 3p\sigma$ transition. In comparison with the frequencies of the ν_2, ν_3 and ν_1 modes for the corresponding ions, these peaks are assigned to

† The digits in parentheses show the vibrational quantum numbers of the ν_1 (C—H stretching), ν_2 (bending) and ν_3 (C≡N stretching) modes. In the present paper the (000) band represents "the (000)←($00^0$0) band".

Table 1
Rydberg transitions in HCN and DCN

Peak [a]	HCN		DCN		Assignment
	$\tilde{\lambda}$ (nm)	$\tilde{\nu}$ ($cm^{-1} \times 10^3$) [b]	$\tilde{\lambda}$ (nm)	$\tilde{\nu}$ ($cm^{-1} \times 10^3$) [b]	
A	121.80	82.10	– [c]	–	$1\pi \rightarrow 3s\sigma$
B	119.11	83.96	– [c]	–	$1\pi \rightarrow 3s\sigma + \nu_3$
C	112.39	88.98	112.14	89.18	$1\pi \rightarrow 3p\sigma$
D	110.91	90.17	110.81	90.25	$1\pi \rightarrow 3p\sigma + 2\nu_2$
E	109.97	90.93	109.89	91.00	$1\pi \rightarrow 3p\sigma + \nu_3$
F	109.24	91.54	109.25	91.54	$5\sigma \rightarrow 3p\sigma$
G	108.62	92.07	108.67	92.02	$1\pi \rightarrow 3p\sigma + \nu_1$
H	107.85	92.72	107.82	92.74	$(5\sigma \rightarrow 3p\pi)$ [d]
I	107.49	93.03	107.54	92.99	$1\pi \rightarrow 3d\sigma$
J	107.13	93.35	106.96	93.49	?
K	≈106.2 [e]	≈94.20	≈106.3 [e]	≈94.07	$1\pi \rightarrow 3d\sigma + 2\nu_2$
L	105.28	94.99	105.15	94.70	$1\pi \rightarrow 3d\sigma + \nu_3$
M	105.06	95.18	105.15	95.10	?
N	104.02	96.14	104.15	96.01	$(5\sigma \rightarrow 3d\sigma)$ [d]
O	102.83	97.25	102.74	97.33	$1\pi \rightarrow 4s\sigma$
P	102.29	97.76	102.26	97.80	$1\pi \rightarrow 4s\sigma + \nu_2$
Q	101.22	98.80	– [f]	–	?
R	100.87	99.13	100.93	99.08	$1\pi \rightarrow 4s\sigma + \nu_3$
S	100.55	99.45	100.57	99.43	$1\pi \rightarrow 4p\sigma$
T	99.44	100.56	99.38	100.63	?
U	98.79	101.23	98.84	101.18	$1\pi \rightarrow 4d\sigma$
V	97.93	102.11	– [f]	–	?
W	97.35	102.72	97.28	102.80	$1\pi \rightarrow 5s\sigma$, $5\sigma \rightarrow 4p\sigma$
X	97.04	103.05	– [f]	–	$1\pi \rightarrow 4d\sigma + \nu_3$
Y	95.78	104.40	95.79	104.39	$1\pi \rightarrow 5d\sigma$, $(5\sigma \rightarrow 4d\sigma)$ [d]
Z	95.04	105.22	94.93	105.34	$1\pi \rightarrow 6s\sigma$
a	94.26	106.09	94.25	106.10	$1\pi \rightarrow 6d\sigma$
b	93.47	106.98	(≈93.6) [g]	(≈106.8)	$5\sigma \rightarrow 5p\sigma$
c	92.80	107.76	(≈92.8) [g]	(≈107.7)	$(5\sigma \rightarrow 5d\sigma)$ [d]
d	92.38	108.25	(≈92.2) [g]	(≈108.4)	?
e	92.02	108.68	– [f]	–	?
f	91.75	109.00	(≈91.7) [g]	(≈109.0)	$5\sigma \rightarrow 6p\sigma$
g	91.08	109.79	91.29	109.54	?

[a] The symbols correspond to those in figs. 2a and 2b.
[b] Experimental errors in the values of $\tilde{\nu}$ are estimated to be 60 cm^{-1}. See section 2.3.
[c] These peaks are diffuse in the DCN spectrum. See section 3.1.1.
[d] Assignments in parentheses are tentative. See section 3.1.4.
[e] These peaks are somewhat diffuse. The wavelengths of these peaks have larger errors than others.
[f] The corresponding peaks are not observed in the DCN spectrum, probably because they are overlapped with other transitions.
[g] In the vicinity of the ionization limits, peaks are weak and overlap each other. Hence the wavelengths in parentheses are less accurate than others.

the (020), (001) and (100) bands, respectively. The frequencies of each mode are about 150 cm^{-1} higher than those of $HCN^+(X^2\Pi)$ or $DCN^+(X^2\Pi)$ ions. Recently, it is proposed [8] that these small peaks may be diffuse vibrational structures appearing in continuous spectra [25, 26].

The (000) band of the $1\pi \rightarrow 3p\sigma$ transition is of high intensity, in comparison with the other vibrational bands of the same member and with

Table 2
Peaks in the 125–110 nm range[a]

Peak[b]	$\tilde{\lambda}$ (nm)	$\tilde{\nu}$ ($cm^{-1} \times 10^3$)[c]
(a) HCN		
α	123.17	81.19
γ	120.90	82.71
δ	≈119.9	≈83.40
ζ	117.87	84.84
η	115.92	86.27
θ	111.36	89.80
(b) DCN		
κ	123.03	81.28
λ	118.64	84.29
μ	≈116.2	≈86.06
ν	114.08	87.66
ξ	112.37	88.99

[a] Well-resolved peaks which possibly constitute vibrational progressions in the 125–110 nm range. The peaks are indicated by arrows in figs. 2a and 2b.
[b] The symbols in part (a) and part (b) of table 2 correspond to those in figs. 2a and 2b, respectively.
[c] Experimental errors in the values of $\tilde{\nu}$ are estimated to be 60 cm^{-1}.

the higher members of this series, $1\pi \rightarrow np\sigma$. This intensity enhancement may result partly from the existence of strong valence transitions in the region of the $1\pi \rightarrow 3p\sigma$ transition.

There have been reported other interpretations for the intense peak C. The corresponding peak observed in the electron energy-loss spectra has been assigned by Tam and Brion [10] to the $1\pi \rightarrow 3p\pi$ transition, while it has been assigned to Åsbrink et al. [12] to the $5\sigma \rightarrow 3p\sigma$ transition having a quantum defect of 0.84. In the present studies, another series of peaks are assigned to the $5\sigma \rightarrow np\sigma$ transitions, as discussed in section 3.1.4.

3.1.3. $1\pi \rightarrow nd\sigma$ series

In the HCN spectrum, a series of intense peaks I, U, Y and a at 107.49, 98.79, 95.78 and 94.26 nm are assigned to the transitions $1\pi \rightarrow 3d\sigma$, $4d\sigma$, $5d\sigma$ and $6d\sigma$, respectively. This series provides a quantum defect of ≈0.44, which is appropriate for the nd series. The corresponding series are also found in the DCN spectrum, as shown in table 1. The (020) and (001) bands of the $n = 3$ member is found in HCN and DCN at about 106 nm.

3.1.4. $5\sigma \rightarrow np\sigma$, $np\pi$ and $nd\sigma$ series

The peak F at 109.24 nm in the HCN spectrum is likely to originate from the first member of the $5\sigma \rightarrow np\sigma$ series because of its sharpness as shown in fig. 2a and is demonstrated in the spectrum of HCN reported by West [4b, 7]. The quantum defect is calculated to be 0.74 on the basis of this assignment; this predicts that the $n = 4$ member is overlapped with a peak of the $1\pi \rightarrow 5s\sigma$ transition and that the peak b at 93.47 nm and the peak f at 91.75 nm can be assigned to the members of $n = 5$ and 6, respectively. In the DCN spectrum, the corresponding members of $n = 5$ and 6 are not well resolved (see table 1). Neither the HCN nor the DCN spectrum has noticeable vibrational members of the $5\sigma \rightarrow np\sigma$ series.

The peak H (107.85 nm for HCN and 107.82 nm for DCN) seems to be ascribable to the $5\sigma \rightarrow 3p\pi$ transition with a quantum defect of 0.67 based on the work of Åsbrink et al. [12]. However, since higher members of this series do not appear clearly in the spectra, the assignments for the $5\sigma \rightarrow np\pi$ series are only tentative.

If the peak N at 104.02 nm in the HCN spectrum is assigned to the $5\sigma \rightarrow 3d\sigma$ transition, the $n = 4$ and 5 members will correspond to the peak Y at 95.78 nm and peak c at 92.80 nm, respectively. However, the peak Y is already assigned to the $1\pi \rightarrow 5d\sigma$ transition as discussed above, and accordingly the present assignments for this series cannot be conclusive.

3.2. Valence transitions

As discussed in previous sections, most of the observed peaks can be assigned to Rydberg transitions. However, there remain several unassigned peaks and broad bands.

A series of small peaks, α, γ, δ and ζ, found in the HCN spectrum are also shown in the absorption spectra reported by West (see fig. 3.4.4 in ref. [4b]) and by Lee [8], whereas no

corresponding peaks are apparent in the electron energy-loss spectra, probably because of their limited energy resolution [10–12]. The asymmetric shape of peak A is indicative of the presence of a tiny peak β on the long wavelength side of peak A. Peak β is more pronounced in the HCN spectrum taken by Lee [10], which has higher resolution. Furthermore, another peak ε is found as an inflection on the short wavelength side of peak B as shown in fig. 2a. These peaks and shoulders, α, β, γ, ε, and ζ, seem to consist of a vibrational progression with a spacing of $\approx$750 cm^{-1} (see fig. 2a). This spacing is comparable with that of the bending mode for the $\tilde{C}$ state of HCN [4a]. In the case of DCN, the corresponding progression which starts at 123.03 nm with a spacing of $\approx$600 cm^{-1} can explain the features in the observed spectrum (see fig. 2b). This spacing is nearly equal to that for the $\tilde{C}$ state of DCN [4a]. These findings show that a valence transition exists at about 120 nm in addition to the $1\pi \rightarrow 3s\sigma$ Rydberg transition. A recent study on quantum yields for the production of CN($B\,^2\Sigma$) from HCN photodissociation supports the existence of this valence state [8]. In the case of HCN, the $(0v_2'0)$ vibrational bands of the $1\pi \rightarrow 3s\sigma$ transition may be superimposed on this vibrational progression. For example, a peak (denoted as δ in our spectrum) appears to have a shoulder in the HCN spectrum by West [4b, 7].

Åsbrink et al. have reported a vibrational progression associated with a $\pi \rightarrow \pi^*$ valence transition with a spacing of $\approx$1450 cm^{-1} in the region centered around 115 nm. It is shown in the present work that the spectrum of HCN in this region differs in shape from that of DCN, probably because of the isotope shifts of their vibrational bands. The corresponding vibrational progressions for HCN and DCN with spacings of $\approx$800 and $\approx$600 cm^{-1}, respectively, appear to exist in this region, as shown in figs. 2a and 2b. However, limited spectral resolution and the intrinsic broadness of these peaks prevent us from furthering the spectral analysis.

In the present analysis, it is not obvious whether the two progressions around 120 and around 115 nm belong to the same electronic transition. Åsbrink et al. have predicted by the HAM/3 method that a $\pi \rightarrow \pi^*$ transition with a $2\,^1\Sigma^+$ upper state is located at 11.2 eV. This calculation was used as a basis for their assignment for the valence transition at about 10.9 eV ($\approx$114 nm) [12]. Recent calculations also show that there are several bound excited states which could correspond to the valence states assigned in the present work [31, 32]. Further theoretical studies of the Rydberg and high-lying valence states will provide a critical test on the existence of the valence transitions at about 120 nm proposed in the present study.

Acknowledgement

The authors wish to thank Professor Yoshitada Murata for his advice in this experiment and Mr. Yoshio Fukuda for his technical help. The measurements were carried out at the Institute for Nuclear Study, The University of Tokyo. We gratefully acknowledge the advice and technical assistance of Mr. Akira Mikuni, Professor Shigemasa Suga and the other members of the Synchrotron Radiation Laboratory of the Institute for Solid State Physics, The University of Tokyo, throughout the measurements. We are also indebted to Professor E. Lindholm and Dr. S. Iwata for their valuable information on the spectral assignments and to Professors Mark S. Gordon and Andrew J. Yencha for their helpful comments and critical reading of the manuscript.

References

[1] H.J. Hilgendorff, Z. Phys. 95 (1935) 781.
[2] G. Herzberg and K.K. Innes, Can. J. Phys. 35 (1957) 842.
[3] G. Herzberg, Molecular spectra and molecular structure, Vol. 3, Electronic spectra and electronic structure of polyatomic molecules (Van Nostrand, Princeton, 1966).

[4] (a) M.T. Macpherson and J.P. Simons, J. Chem. Soc. Faraday II 74 (1978) 1965;
(b) M.N.R. Ashfold, M.T. Macpherson and J.P. Simons, in: Topics in current chemistry, Vol. 86, Spectroscopy (Springer, Berlin, 1979).
[5] W.C. Price, Phys. Rev. 46 (1934) 529.
[6] W.C. Price and A.D. Walsh, Trans. Faraday Soc. 41 (1945) 381.
[7] G.A. West, Ph.D. Thesis, Wisconsin (1975).
[8] L.C. Lee, J. Chem. Phys. 72 (1980) 6414.
[9] A. Chutjian, H. Tanaka, B.G. Wicke and S.K. Srivastava, J. Chem. Phys. 67 (1977) 4835.
[10] W.-C. Tam and C.E. Brion, J. Electron Spectry. 3 (1974) 281.
[11] C. Fridh and L. Åsbrink, J. Electron Spectry. 7 (1975) 119.
[12] L. Åsbrink, C. Fridh and E. Lindholm, Chem. Phys. 27 (1978) 159;
E. Lindholm, private communication (November, 1979).
[13] A.P. Hitchcock and C.E. Brion, Chem. Phys. 37 (1979) 319.
[14] J.A.R. Samson, Techniques of vacuum ultraviolet spectroscopy (Wiley, New York, 1967).
[15] G. Bauer, Handbook of preparative inorganic chemistry, Vol. 1 (Academic Press, New York, 1963).
[16] Y. Tanaka, A.S. Jursa and F.J. LeBlanc, J. Chem. Phys. 32 (1960) 1205.
[17] W.C. Price, Phys. Rev. 47 (1935) 444.
[18] T. Nakayama and K. Watanabe, J. Chem. Phys. 40 (1964) 558.
[19] A.D. McLean, J. Chem. Phys. 37 (1962) 627.
[20] W.E. Palke and W.N. Lipscomb, J. Am. Chem. Soc. 88 (1966) 2384.
[21] D.C. Pan and L.C. Allen, J. Chem. Phys. 46 (1967) 1797.
[22] J.-B. Robert, H. Marsmann, I. Absar and J.R. Van Wazer, J. Am. Chem. Soc. 93 (1971) 3320.
[23] D.C. Frost, S.T. Lee and C.A. McDowell, Chem. Phys. Letters 23 (1973) 472.
[24] A.B.F. Duncan, Rydberg series in atoms and molecules (Academic Press, New York, 1971).
[25] R.T Pack, J. Chem. Phys. 65 (1976) 4765.
[26] E.J. Heller, J. Chem. Phys. 68 (1978) 3891.
[27] G.M. Schwenzer, S.V. O'Neil, H.F. Schaefer III, C.P. Baskin and C.F. Bender, J. Chem. Phys. 60 (1974) 2787.
[28] G.M. Schwenzer, C.F. Bender and H.F. Schaefer III, Chem. Phys. Letters 36 (1975) 179.
[29] M. Perić, S.D. Peyerimhoff and R.J. Buenker, Can. J. Chem. 55 (1977) 3664.
[30] G.J. Vazquez and J.F. Gouyet, Chem. Phys. Letters 57 (1978) 385.
[31] G.J. Vazquez and J.F. Gouyet, Chem. Phys. Letters 65 (1979) 515.
[32] J. Hay, private communication (September, 1980).